ACS Catalysis

Research Article

pubs.acs.org/acscatalysis

# Hydrogenation of Carbon Dioxide Using Half-Sandwich Cobalt, Rhodium, and Iridium Complexes: DFT Study on the Mechanism and Metal Effect

Cheng Hou, Jingxing Jiang, Shidong Zhang, Guo Wang, Zhihan Zhang, Zhuofeng Ke,* and Cunyuan Zhao*

MOE Key Laboratory of Bioinorganic and Synthetic Chemistry/KLGHEI of Environment and Energy Chemistry, School of Chemistry and Chemical Engineering, Sun Yat-sen University, Guangzhou, 510275 Guangdong, P. R. China

Supporting Information

**ABSTRACT:** The hydrogenation of carbon dioxide catalyzed by half-sandwich transition metal complexes (M = Co, Rh, and Ir) was studied systematically through density functional theory calculations. All metal complexes are found to process a similar mechanism, which involves two main steps, the heterolytic cleavage of $H_2$ and the hydride transfer. The heterolytic cleavage of $H_2$ is the rate-determining step. The comparison of three catalytic systems suggests that the Ir catalyst has the lowest activation free energy (13.4 kcal/mol). In contrast, Rh (14.2 kcal/mol) and Co (18.3 kcal/mol) catalysts have to overcome relatively higher free energy barriers. The different catalytic efficiency of Co, Rh, and Ir is attributed to the back-donation ability of different metal centers, which significantly affects the $H_2$ heterolytic cleavage. The highest activity of an iridium catalyst is attributed to its strong back-donation ability, which is described quantitatively by the second order perturbation theory analysis. Our study indicates that the functional group of the catalyst plays versatile roles on the catalytic cycle to facilitate the reaction. It acts as a base (deprotonated) to assist the heterolytic cleavage of $H_2$. On the other hand, during the hydride transfer, it can also serve as Brønsted acid (protonated) to lower the LUMO of $CO_2$. This ligand assisted pathway is more favorable than the direct attack of hydride to $CO_2$. These finds highlight that the unique features of the metal center and the functional ligands are crucial for the catalyst design in the hydrogenation of carbon dioxide.

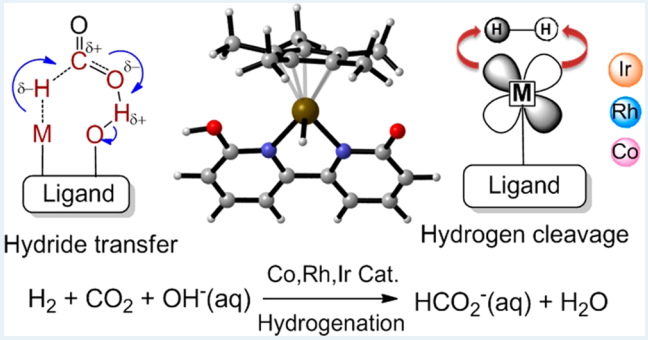


$$H_2 + CO_2 + OH^-(aq) \xrightarrow[\text{Hydrogenation}]{\text{Co,Rh,Ir Cat.}} HCO_2^-(aq) + H_2O$$

**KEYWORDS:** *carbon dioxide, hydrogenation, iridium, rhodium, cobalt, catalytic mechanism, metal effect, density functional theory*

## 1. INTRODUCTION

With the rapid industrialization over the last century, the energy crisis, caused by the overconsumption of fossil fuel, has become a vital problem for human beings. On the other hand, the combustion of fossil fuel leads to the excessive emission of carbon dioxide, which is the main reason for global warming.[1] Therefore, great efforts have been made by scientists to find sustainable, clean energy which can also help reduce the emission of carbon dioxide. Among all the proposed methods, the interconversion of carbon dioxide and formic acid has received considerable attention.[2] Besides the advantages of formic acid such as low toxicity and high density of energy (4.4 wt %),[3] the overall formation energy of formic acid's formation is rather low (eq 1; $\Delta G^o = -4$ kJ/mol in water).[4] Therefore, formic acid is considered as a promising hydrogen carrier.

$$H_2 + CO_2 + OH^-(aq) \rightleftharpoons HCO_2^-(aq) + H_2O \quad (1)$$

A number of homogeneous catalysts with high catalytic activity for the hydrogenation of carbon dioxide to formic acid were reported over the past few years. Significantly, Nozaki and co-workers reported an unprecedented high activity with a turnover number (TON) of 3 500 000 and a turnover frequency (TOF) of 150 000 $h^{-1}$ by an iridium catalyst, and they proposed the PNP ligand (PNP stands for 2,6-bis-dialkylphosphinomethyl-pyridine) participated the $H_2$ heterolytic cleavage through a dearomatization process.[5] The following mechanistic study by Ahlquist[6] and Yang[7] suggested that the PNP ligand of the second coordination sphere was not able to participate in the $H_2$ heterolytic cleavage through a dearomatization process, and the heterolytic cleavage was promoted by an external base. Later, Nozaki and co-workers carried out a more detailed mechanistic study, and the result indicated that both the dearomatization mechanism and the external base induced mechanism operated concurrently in this system.[5a] A comparable activity (Maximum TON of 348 000) was also reached with an iridium hydride complex prepared by

Received: May 21, 2014
Revised: July 24, 2014
Published: July 28, 2014

   dx.doi.org/10.1021/cs500688q | ACS Catal. 2014, 4, 2990−2997

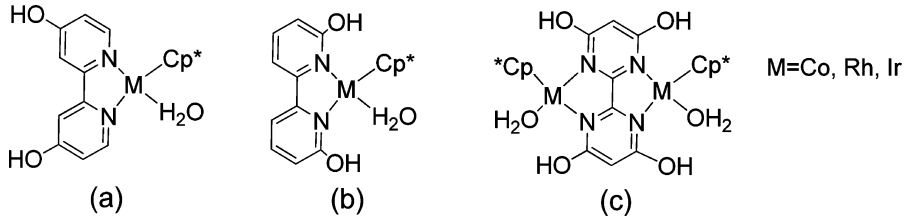


**Figure 1.** Typical half-sandwich complexes for hydrogenation of carbon dioxide.

Hazari et al.[8] The high catalytic efficiency is attributed to the energy barrier lowered by the hydrogen-bond donor in the second coordination sphere. Besides the catalyst based on noble metal, there is a shift for the catalyst metal center from noble metals (Rh, Ir, and Ru) to earth abundant metals (Fe, Co, and Ni) for a long time.[9] With a combinatorial catalyst screening device, Jessop et al. achieved a TOF of 15 $h^{-1}$ using $FeCl_3$ and $NiCl_3$ with phosphine ligand.[10] Another breakthrough was made by Beller et al. using an iron complex with a "tetraphos" ($P(CH_2CH_2PPh_2)_3$) ligand.[11] Later, they extended the range of metal center to cobalt. An excellent activity (TOF of 195 $h^{-1}$ and TON of 3 877) was obtained by a cobalt dihydride complex, which is comparable with many noble metal systems.[12] With the same PNP pincer backbone of Nozaki's catalyst, Milstein et al. developed an iron catalyst which exhibited excellent catalytic efficiency (TOF of 156 $h^{-1}$ and TON of 788 under low pressure of 6.6 atm for $H_2$ and 3.3 atm for $CO_2$).[13] The proposed mechanism was similar to the former computational study by Yang.[7] By successfully matching the thermodynamic parameters such as the metal hydricity and $pK_a$,[14] Appel et al. developed a $CO_2$ hydrogenation system by a cobalt hydride complex.[15] The catalytic activity is comparable to the highest iridium catalyst (TOF of 3 400 $h^{-1}$ at room temperature in THF at 1 atm). Later, they performed a detailed computational study to illuminate the catalytic mechanism.[16] The result suggested the precoordination of $CO_2$ to Co was the rate-determining step, and the associative pathway was more favored than the direct hydride transfer pathway.

Besides the catalysts which all have phosphine ligands mentioned above, another approach to $CO_2$ hydrogenation was achieved by a half-sandwich catalyst $[Cp^*M\ (4,4'\text{-}R_2\text{-bpy})(OH_2)]^{2+}$ (M = Co, Rh, Ir, bpy = 2,2′-bipyridine, R = OH) (Figure 1a) developed by Himeda et al.[17] Later, the hydroxyl group on the bipyridine ligand was moved to the ortho-position $[Cp^*M\ (6,6'\text{-}R_2\text{-bpy})(OH_2)]^{2+}$ (M = Co, Rh, Ir, bpy = 2,2′-bipyridine, R = OH) (Figure 1b) to provide a second coordination sphere by acting as a pendent base to participate the heterolytic cleavage of $H_2$, which is considered to accelerate the RDS (rate-determining step). Unlike other catalysts which require high pressure and temperature, the most active dinuclear iridium catalyst $[(Cp^*IrOH_2)_2(THBPM)]^{2+}$ (THBPM = 4,4′,6,6′-tetrahydroxyl-4,4′- bipyrimidine) (Figure 1c) exhibited an excellent activity with a turnover frequency of 70 $h^{-1}$ under mild conditions (25 °C and 1 atm $H_2/CO_2$).[18] Moreover, it can be used both in the hydrogenation of $CO_2$ and the decomposition of formic acid through different experimental conditions.

Although the catalysts developed by Himeda are based on the same backbone, a different metal center even in the same group leads to a huge difference in catalytic activity. As for the group 9 transitional metals, the iridium catalyst shows the highest activity with an initial TOF of 5 100 $h^{-1}$ at 80 °C and 1 MPa of $H_2/CO_2$ among others (160 $h^{-1}$ at 80 °C and 1 MPa of $H_2/CO_2$ for Rh, 1.3 $h^{-1}$ at 50 °C and 4 MPa of $H_2/CO_2$ for Co).[17a,19] On the other hand, former calculation only involved one pathway. Some important intermediates and transition states are still missing. Why is iridium the best metal center? What role did the metal effect play in the $CO_2$ hydrogenation system? Are there other reaction pathways in the catalytic cycle? In order to shed light on these important questions, a theoretical study based on density functional theory (DFT) is performed. Focusing on group 9 transition metals, the metal effect is discussed systematically with the NBO (natural bond orbital) method. Both inner sphere and outer sphere mechanisms are summarized and compared. This theoretical investigation presented here is expected to provide useful information for future catalyst design.

## 2. COMPUTATIONAL DETAILS

All the structures were fully optimized at the B3LYP[20]/BSI level (BSI designated the basis set combination of CEP-121g[21] for metal atom and 6-31G (d, p) for nonmetal atoms). Frequency analysis calculations were performed to characterize the structures to be the minima or transition states. IRC calculations were adopted to confirm the connection of the transition states and two relevant minima. At B3LYP/BSI optimized geometries, the free energy results were refined by calculating the single point energy at the B3LYP/BSII level (BSII designated CEP-121g for metal atoms and 6-311++g (d, p) for nonmetal atoms) with solvation effect. The solvent, water, was simulated with the SMD[22] continuum model at the B3LYP/BSII level. An additional correction (1.89 kcal/moll) was added to the free energy term for converting the standard free energy of ideal gas to the standard state of the solution.[23] All the calculations were performed with the Gaussian 09 program.[24] Natural bond orbital (NBO[25]) calculation was carried out for the electron population analysis and second order perturbation theory analysis. The free energy results were adjusted to experimental condition, pH = 8.3, based on the equation $\Delta G = RT \ln(Q/K_{eq})$.[26] The 3D optimized structure figures in this paper were drawn by the Sylvie visualization program.[27]

## 3. RESULTS AND DISCUSSION

**3.1. The Reaction Mechanism.** The overall mechanism consists of two steps, the heterolysis cleavage of the $H_2$ and the hydride transfer to the $CO_2$. Former research indicated that the heterolysis cleavage step involved a water molecule acting as a bridge, which is verified by computational methods and isotope labeling methods.[26] Herein, we chose this transition mode to compare the activity of different metals. As for the hydride transfer step, four possible pathways were proposed according to former mechanism study on the polar bond hydrogenation.[28] Both inner sphere pathway and outer sphere pathway are involved. There are two possible transition states for each part (see Figure 2). For the inner sphere, the Cp* (pentamethyl-


dx.doi.org/10.1021/cs500688q | ACS Catal. 2014, 4, 2990−2997

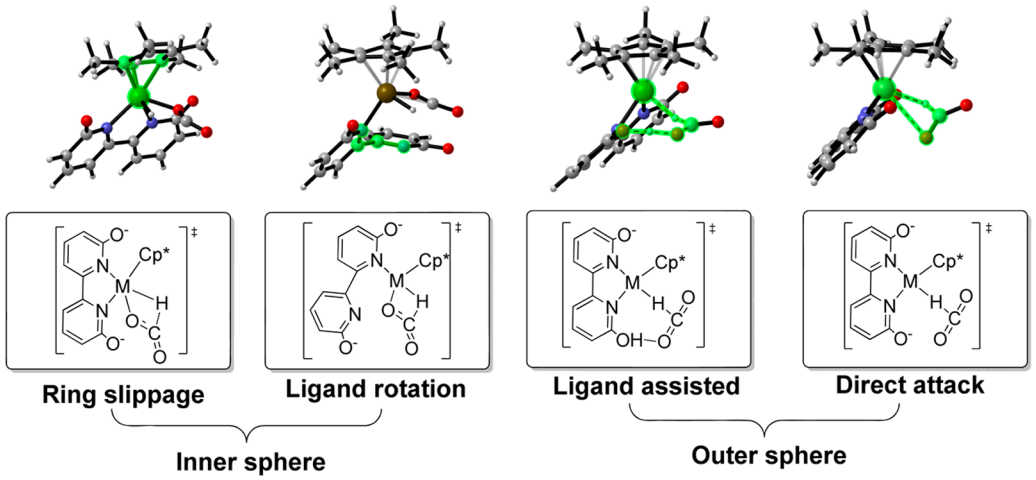


**Figure 2.** Four possible pathways of hydride transfer.

**Scheme 1. Catalytic Cycle for the Hydrogenation of Carbon Dioxide through Outer Sphere Process**

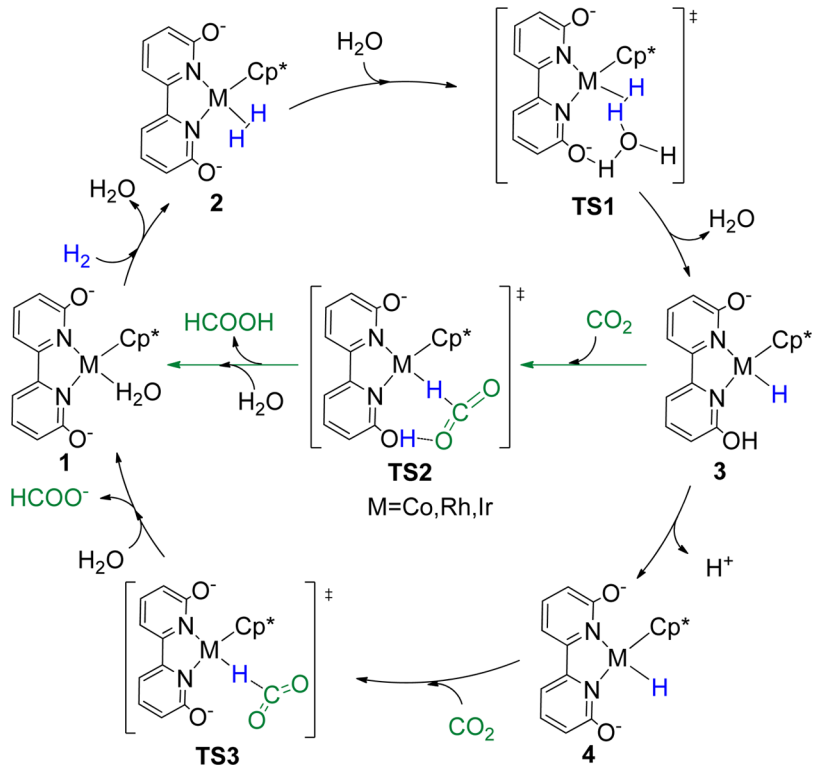


cyclopentadiene) ring may slip[29] and become a $\eta-3$ coordinated mode to provide a vacant site on the metal for the carbon dioxide to coordinate. Another situation is the bpy (2,2′-bipyridine) group may have a rotation to provide a vacant site for carbon dioxide. However, none of these intermediates through the two processes can be located by the computational method. This can be attributed to the relatively high energetic penalty of losing conjugation. Thus, the inner sphere hydrogenation is unlikely to happen in this system. Finally, the outer sphere was chosen for this research.

As for the outer sphere, direct hydride transfer to $CO_2$ is taken into consideration. A former calculation study indicated that the $CO_2$ insertion into the M−H bond is very late and is nearly at the geometry of formate.[30] Due to the pendent hydroxyl group providing a second coordination sphere interaction, another pathway which has a ligand assisted hydride transfer is proposed. The metal hydride and the proton of the hydroxyl group will transfer to $CO_2$ synchronously before deprotonated. The overall proposed catalytic cycle is presented in Scheme 1.

The overall potential energy surface is presented in Figure 3. The catalytic cycle mainly consists of two steps: the heterolytic cleavage of $H_2$ and the hydride transfer. Complex **1** with a solvated water molecule was chosen as the starting point. During the catalysis, the coordinated water molecule will be exchanged with the reactant, hydrogen molecule, to form a $H_2$ $\sigma$-complex **2**. A comparison of the formation of $H_2$ $\sigma$-complexes for Co, Rh, and Ir indicates that the formation of **Ir-2** is a downhill step in free energy (−2.4 kcal/mol), different from the formation of **Rh-2** and **Co-2**, which are slightly uphill by 0.1


dx.doi.org/10.1021/cs500688q | ACS Catal. 2014, 4, 2990−2997

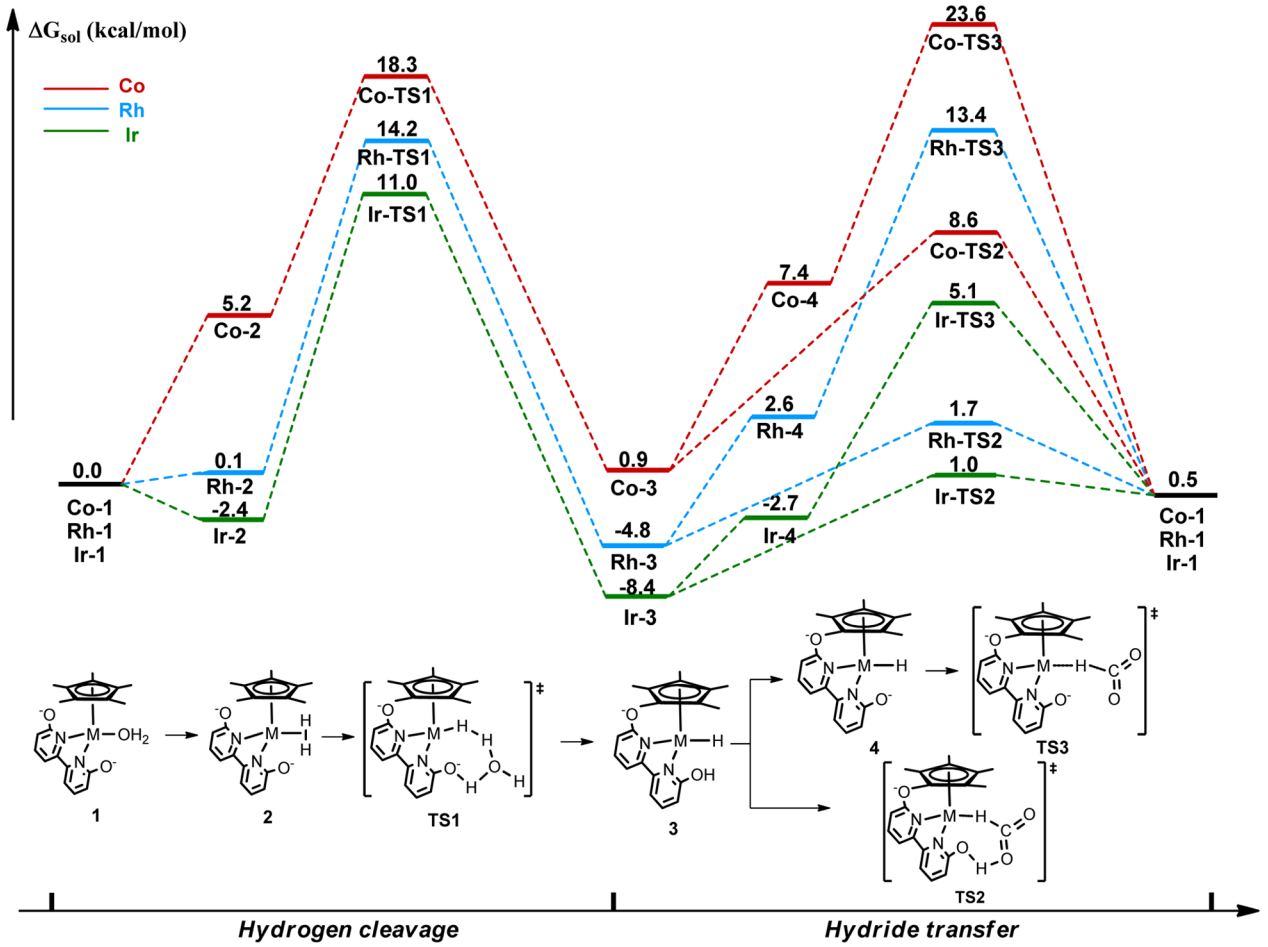


**Figure 3.** Free energy profile of the catalytic cycle shown in Scheme 1. Optimized at the B3LYP/BSI B3LYP/BSII (SMD, solvent = water) level of theory.

and 5.2 kcal/mol, respectively. After the coordination of $H_2$, the oxygen anion of the bpy ligand assists the heterolytic cleavage of $H_2$ with a bridge-like water molecular to form the hydroxyl group and metal hydride. The calculated activation free energies barrier for Co, Rh, and Ir catalysts are 18.3, 14.2, and 13.4 kcal/mol, respectively. Our calculation indicates that the iridium catalyst has the lowest activation barrier for hydrogen heterolytic cleavage, which agrees to the experimental observation on the catalytic activity order of the different metal center. In order to further confirm the calculated result, KIE calculation was performed including Wigner's tunneling effect correction. The result is inconsistent with the experimental observed KIE values (see Table S4).

The metal hydride intermediate **3** is formed after the heterolytic cleavage. The relative free energy of **Ir-3** is −8.4 kcal/mol, which indicates that the formation of iridium-hydride is the most thermodynamically favored compared to the formation of **Rh-3** (−4.8 kcal/mol) and **Co-3** (0.9 kcal/mol). The subsequent hydride transfer to carbon dioxide from metal hydride can proceed through two possible pathways: the direct attack on carbon dioxide after the deprotonation of hydroxyl or the assisted hydride transfer with the aid of hydroxyl. Our study reveals that the ligand assisted hydride transfer goes through a six-membered ring transition state **TS2** with very low free energy barriers, with the calculation result of 7.7, 6.5, and 9.4 kcal/mol for Co, Rh, and Ir, respectively. On the contrary, the direct attack of the hydride to $CO_2$ has to overcome a much higher activation free energy. The deprotonated intermediates **4** are uphill by 6.5 kcal/mol, 7.4 kcal/mol, and 5.7 kcal/mol for Co, Rh, and Ir, respectively. The located transition states **TS3** are rather high in free energy (5.1, 13.4, and 23.6 kcal/mol for **Ir-TS3**, **Rh-TS3**, and **Co-TS3**, respectively) as compared to the ligand assisted hydride transfer transition state **TS2**. The water involved hydride transfer mode (see Figure S1) for **TS2** and **TS3** is also considered (see Table S1 in the SI). However, the results indicate that this eight member ring mode is quite disfavored due to the ring strain and extra entropy penalty. We further evaluated the dispersion effect on our investigated systems. The DFT dispersion results are similar to the B3LYP results, leading to the same energetic trend and conclusion (see Table S3). To better evaluate the free energy change of the deprotonation process, the relative free energy of **4** and **TS3** were calculated with the experimental solvation free energy of proton ($G_{solv}$ ($H^+$) = −272.18 kcal/mol),[31] which has been used successfully in a similar research.[32] The Rh catalyst shows the best hydride transfer ability with an energy barrier of 6.5 kcal/mol, which is in agreement with a former study on metal hydricity comparison.[14a] After hydride transfer, the formic acid is formed and the catalyst regenerates.

**3.2. The Origin of the Metal Effects.** From the energy profile in Figure 3 shown above, we can see that all the metal complexes are found to proceed via a similar mechanism. Among the main steps of the catalytic cycle, the heterolytic cleavage of $H_2$ is the rate-determining step. The overall free


dx.doi.org/10.1021/cs500688q | ACS Catal. 2014, 4, 2990−2997

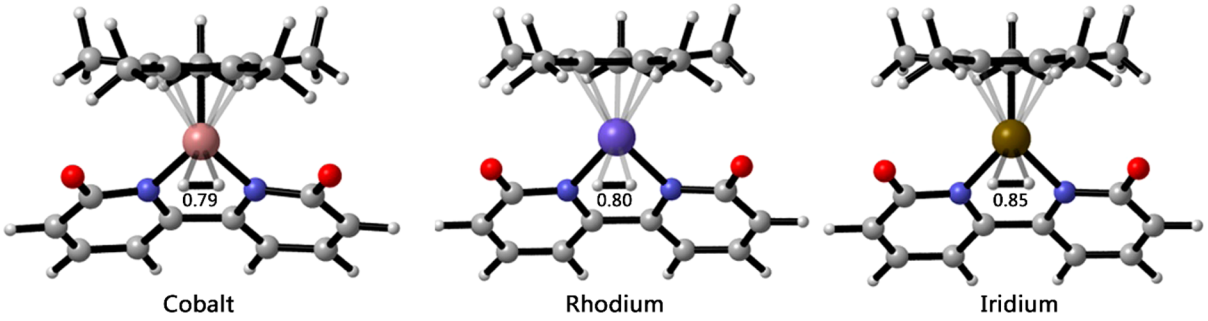


**Figure 4.** Optimized structures of **Co-2**, **Rh-2**, and **Ir-2**. The distances are in Å.

energy barrier of each metal is 18.3, 14.2, and 13.4 kcal/mol for Co, Rh, and Ir, respectively. The iridium catalyst has the lowest activation free energy and is predicted to be the most active catalyst, which agrees with the experimental observation.

Then we turn to analyze the origin of the metal effects. As we can see from the calculated energy profile, the heterolytic cleavage of $H_2$ is the rate-determining step. It starts from the $H_2$ $\sigma$-complex **2**. As shown in Figure 4, we can see the $H_2$ bond length of the $H_2$ $\sigma$-complex increases along with the atomic number. The H−H bond distance of the coordinated $H_2$ in **Ir-2** is lengthened by 0.11 Å compared to the standard dihydrogen bond length (0.74 Å). The H−H bond lengths of **Co-2** and **Rh-2** complexes are also elongated to a less degree (by 0.05 and 0.06 Å, respectively). Ever since Kubas[33] and co-workers discovered the first $H_2$ complex $W(CO)_3$-$(P^iPr_3)_2(H_2)$, numerous stable $H_2$ complexes have been synthesized and characterized by spectroscopic methods.[34] Intriguing experimental observation shows that the coordinated $H_2$ molecular can be lengthened by around 0.06 Å after coordination. This fact can be well explained by molecular orbital theory. As shown in Figure 5, the bonding electron pair of the hydrogen

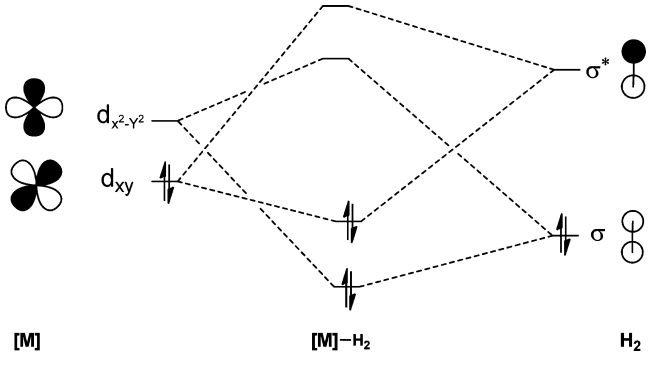


**Figure 5.** Orbital interaction of $H_2$ complex.

molecular will fill the empty d orbital through an M-$\eta^2$-$H_2$ coordination structure, and the filled d orbital will interact with the antibonding electron pair to provide a back-donation for the $H_2$. Thus, the bond order of $H_2$ will be lowered and the bond length will be elongated. The metal center can use this back-donation effect to activate the $H_2$ molecular and facilitate the heterolytic cleavage, which is the rate-determining step of the catalytic cycle in this system.

In order to evaluate the back-donation ability of different metal center, the NBO (natural bond orbital) analysis was employed to perform second order perturbation theory analysis. It shows that the second order stabilization energy of iridium from the iridium $d_{xy}$ orbital to the $H_2$ $\sigma^*$ antibonding orbital is 22.24 kcal/mol, which is more than twice the energy of rhodium (8.42 kcal/mol) and more than six times of cobalt (3.56 kcal/mol). The stabilization energy for cobalt catalyst is less than 5 kcal/mol, which lacks significant back-donation effect. The calculated result indicates that the iridium has the greatest d orbital back-donation ability compared with rhodium and cobalt, which well explains the experimental observed catalytic order (Table 1). It can be concluded that the coordinated $H_2$ on the iridium complex is well activated by the back-donation of the iridium and leads to the high catalytic activity. This kind of back bonding from the d orbital of the metal to the $\sigma^*$ orbital of $H_2$ can be seen from the Kohn−Sham orbitals of complexes **Co-2**, **Rh-2**, and **Ir-2** (Figure 6).Although former studies tended to explain the catalytic activity difference through the perspective of thermal stability of the catalysts, the back-donation of metal is also an important factor which cannot be ignored for activating the hydrogen molecule.

**3.3. Versatile Roles of Functional Group on the Catalytic Mechanism.** With the understanding of the role of functional group as a pendent base ($O^-$) to assist the heterolytic cleavage of $H_2$, we then analyze how the functional group facilitated the hydride transfer step. As shown in Figure 7, two possible pathways were evaluated in our studies, i.e., the direct attack of hydride to carbon dioxide with a functional group at a deprotonated anion state ($O^-$) and the assisted hydride transfer with the aid of a functional group at a protonation state (OH). Analysis of the hydroxyl assisted hydride transfer transition states suggests two important factors can account for the reaction facilitation. The hydroxyl group acts as a Brønsted acid to form a hydrogen bond with the oxygen atom on the carbon dioxide, which will 1) stabilize the transition state by a six-member ring and 2) will participate the distribution of electron when the hydride attacks the carbon atom. The origin of these stabilizations can be explained by

**Table 1. Second Order Perturbation Theory Analysis Results for Complexes 2 and Experimental Catalytic Activity**

| metal | E(2) kcal/mol ($d_{xy} \rightarrow \sigma^*$) | bond length (H−H) | TOF ($h^{-1}$) | $T$ (°C) | ref |
|---|---|---|---|---|---|
| Ir | 22.24 | 0.85 | 5100 | 80 | 17a |
| Rh | 8.42 | 0.80 | 160 | 80 | 17a |
| Co | 3.56 | 0.79 | 1.3 | 50 | 19 |


dx.doi.org/10.1021/cs500688q | ACS Catal. 2014, 4, 2990−2997

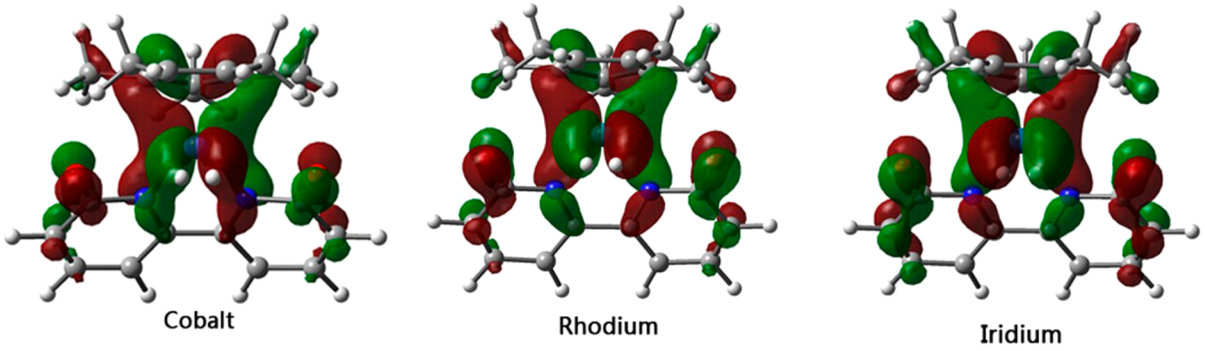


**Figure 6.** Kohn–Sham orbitals of the back bonding from the metal d orbital to the $H_2$ $\sigma^*$ orbital (isovalue = 0.02).

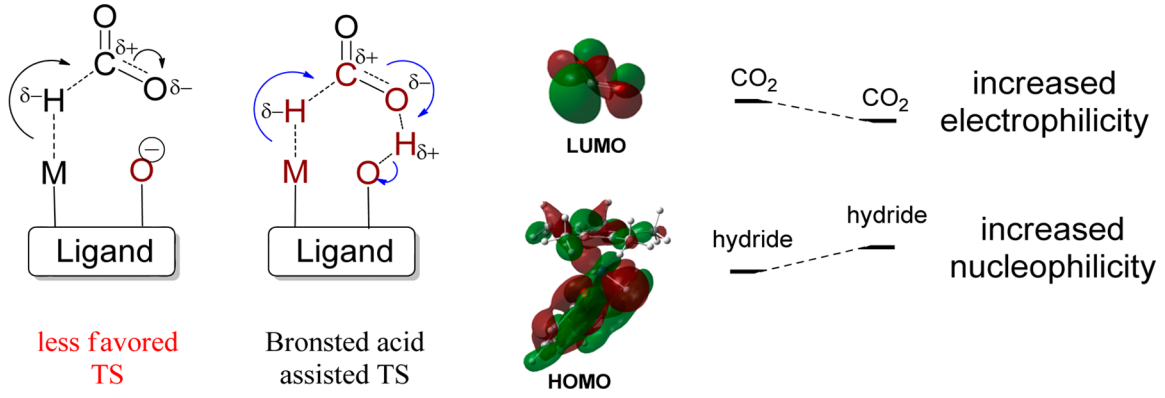


**Figure 7.** Roles of the functional group in assisting hydride transfer (The Kohn–Sham orbitals of the LUMO of bent $CO_2$ and the HOMO of the hydride complex; isovalue = 0.02).

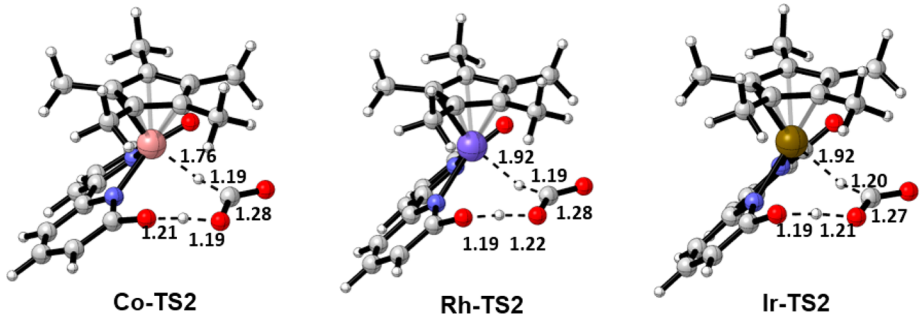


**Figure 8.** Optimized structures of the ligand-assisting attack on carbon dioxide **TS2** (Co-TS2: 665*i* $cm^{-1}$, Rh-TS2: 700*i* $cm^{-1}$, Ir-TS2: 765*i* $cm^{-1}$). The distances are in Å.

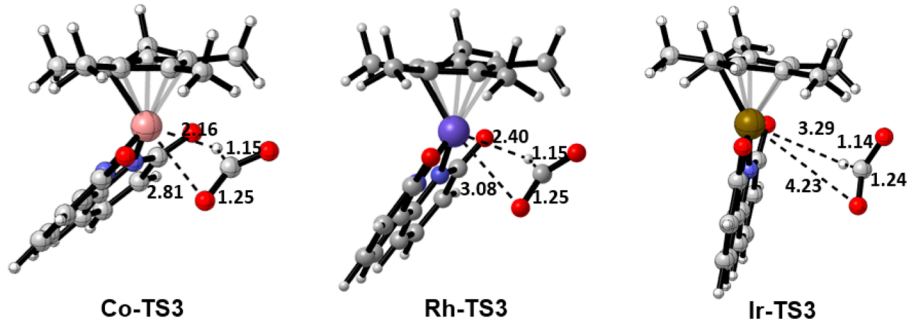


**Figure 9.** Optimized structures of the direct attack on carbon dioxide **TS3** (Co-TS3: 407*i* $cm^{-1}$, Rh-TS3: 332*i* $cm^{-1}$, Ir-TS2: 186*i* $cm^{-1}$). The distances are in Å.

frontier molecular orbital interactions (Figure 7). The hydroxyl group acts as a Brønsted acid to lower the LUMO of carbon dioxide by H-bonding, resulting in an increased electrophilicity of $CO_2$. On the other hand, the H-bonding redistributes the electron density. The breaking of hydroxyl O–H bond will increase the electron density of bpy ligand and enhance the


dx.doi.org/10.1021/cs500688q | ACS Catal. 2014, 4, 2990–2997

nucleophilicity of metal-hydride. We use the NBO charge distribution to compare the electrophilicity of $CO_2$ between **TS2** (Figure 8) and **TS3** (Figure 9). As listed in Table 2, the

**Table 2. NBO Charge on the Electrophilic Carbon Atom of $CO_2$ in TS2 and TS3**

| metal | Co | Rh | Ir |
|---|---|---|---|
| **TS2** | 0.763 | 0.736 | 0.759 |
| **TS3** | 0.630 | 0.618 | 0.622 |

charge distribution on the carbon atom of $CO_2$ in **TS3** is +0.630, +0.618, and +0.622 for Co, Rh, and Ir, respectively, which is less electrophilic than **TS2** (+0.763, +0.736, and +0.759 for Co, Rh, and Ir, respectively). The result is consistent with the calculated PES, and the TS2 is significantly lowered by the hydroxyl group. All the carbon atoms of $CO_2$ in **TS2**s are more electrophilic than **TS3**s because of the ligand assistance. We also located another **TS2′** with the proton remaining on the hydroxyl group. However, **TS2′** is slightly higher than **TS2** (∼5 kcal/mol) in free energy. Therefore, the synergetic increased electrophilicity of $CO_2$ and enhanced nucleophilicity of metal-hydride made TS2 a transition state with lower free energies than TS3; the functional group serves as a Brønsted acid (in protonated form) to lower the LUMO of $CO_2$ and facilitates the hydride transfer.

## 4. CONCLUSION

In summary, a detailed study of the carbon dioxide hydrogenation reaction using a half-sandwich transition metal complex $[Cp^*M\ (6,6'\text{-}R_2\text{-bpy})(OH_2)]^{2+}$ (M = Co, Rh, Ir, bpy = 2,2′-bipyridine, R = OH) as the catalyst is presented. The catalytic cycle involves two aspects: the heterolytic cleavage of $H_2$ and the hydride transfer process. The result indicates the heterolytic cleavage is the rate-determining step of the whole catalytic cycle. The differences in the catalytic activity of cobalt, rhodium, and iridium are mainly attributed to the different d orbital back-donation ability of each metal. The NBO analysis was employed to verify the back-donation ability of different metals. The calculated result agreed with the experimental observation on the catalytic activity order of different metals. As for the hydride transfer step, it will proceed through an outer sphere ligand assisted mechanism. This is because the hydroxyl group may act as a Brønsted acid to lower the LUMO of $CO_2$ along with the ability to increase the HOMO of the metal hydride during hydride transfer. The unique effect of the metal center and the versatile function of the ligand of the second coordination sphere play important roles both in the hydrogen activation process and the hydrogenation reaction process. These theoretical results are presented as a rational guidance of catalyst design in the future.

## ■ ASSOCIATED CONTENT

### Supporting Information

Complete ref 24, other hydride transfer modes, energetic summary for all structures, dispersion effect, KIE calculations, and Cartesian coordinates of all optimized structures. This material is available free of charge via the Internet at http://pubs.acs.org.

## ■ AUTHOR INFORMATION

### Corresponding Authors

*E-mail: kezhf3@mail.sysu.edu.cn.

*E-mail: ceszhcy@mail.sysu.edu.cn.

### Notes

The authors declare no competing financial interest.

## ■ ACKNOWLEDGMENTS

This work was supported by the NSFC funding (Grants 21203256, 21173273, 21373277, and J1103305). Computing facilities were supported in part by the high performance grid computing platform of Sun Yat-sen University, the Guangdong Province Key Laboratory of Computational Science, and the Guangdong Province Computational Science Innovative Research Team.

## ■ REFERENCES

(1) Appel, A. M.; Bercaw, J. E.; Bocarsly, A. B.; Dobbek, H.; DuBois, D. L.; Dupuis, M.; Ferry, J. G.; Fujita, E.; Hille, R.; Kenis, P. J. A.; Kerfeld, C. A.; Morris, R. H.; Peden, C. H. F.; Portis, A. R.; Ragsdale, S. W.; Rauchfuss, T. B.; Reek, J. N. H.; Seefeldt, L. C.; Thauer, R. K.; Waldrop, G. L. *Chem. Rev.* **2013**, *113*, 6621−6658.

(2) Johnson, T. C.; Morris, D. J.; Wills, M. *Chem. Soc. Rev.* **2010**, *39*, 81−88.

(3) Grasemann, M.; Laurenczy, G. *Energy Environ. Sci.* **2012**, *5*, 8171−8181.

(4) Jessop, P. G.; Joó, F.; Tai, C. C. *Coord. Chem. Rev.* **2004**, *248*, 2425−2442.

(5) (a) Tanaka, R.; Yamashita, M.; Chung, L. W.; Morokuma, K.; Nozaki, K. *Organometallics* **2011**, *30*, 6742−6750. (b) Tanaka, R.; Yamashita, M.; Nozaki, K. *J. Am. Chem. Soc.* **2009**, *131*, 14168−14169.

(6) Ahlquist, M. S. G. *J. Mol. Catal. A: Chem.* **2010**, *324*, 3−8.

(7) Yang, X. Z. *ACS Catal.* **2011**, *1*, 849−854.

(8) Schmeier, T. J.; Dobereiner, G. E.; Crabtree, R. H.; Hazari, N. *J. Am. Chem. Soc.* **2011**, *133*, 9274−9277.

(9) Inoue, Y.; Izumida, H.; Sasaki, Y.; Hashimoto, H. *Chem. Lett.* **1976**, 863−864.

(10) Tai, C. C.; Chang, T.; Roller, B.; Jessop, P. G. *Inorg. Chem.* **2003**, *42*, 7340−7341.

(11) Federsel, C.; Boddien, A.; Jackstell, R.; Jennerjahn, R.; Dyson, P. J.; Scopelliti, R.; Laurenczy, G.; Beller, M. *Angew. Chem.* **2010**, *122*, 9971−9974.

(12) Federsel, C.; Ziebart, C.; Jackstell, R.; Baumann, W.; Beller, M. *Chem.—Eur. J.* **2012**, *18*, 72−75.

(13) Langer, R.; Diskin Posner, Y.; Leitus, G.; Shimon, L. J. W.; Ben-David, Y.; Milstein, D. *Angew. Chem., Int. Ed.* **2011**, *50*, 9948−9952.

(14) (a) Qi, X. J.; Fu, Y.; Liu, L.; Guo, Q. X. *Organometallics* **2007**, *26*, 4197−4203. (b) Qi, X. J.; Liu, L.; Fu, Y.; Guo, Q. X. *Organometallics* **2006**, *25*, 5879−5886.

(15) Jeletic, M. S.; Mock, M. T.; Appel, A. M.; Linehan, J. C. *J. Am. Chem. Soc.* **2013**, *135*, 11533−11536.

(16) Kumar, N.; Camaioni, D.; Dupuis, M.; Raugei, S.; Appel, A. M. *Dalton. Trans.* **2014**, 11803−11806.

(17) (a) Himeda, Y.; Miyazawa, S.; Hirose, T. *ChemSusChem* **2011**, *4*, 487−493. (b) Himeda, Y.; Onozawa-Komatsuzaki, N.; Sugihara, H.; Kasuga, K. *Organometallics* **2007**, *26*, 702−712.

(18) Hull, J. F.; Himeda, Y.; Wang, W. H.; Hashiguchi, B.; Periana, R.; Szalda, D. J.; Muckerman, J. T.; Fujita, E. *Nat. Chem.* **2012**, *4*, 383−388.

(19) Badiei, Y. M.; Wang, W.-H.; Hull, J. F.; Szalda, D. J.; Muckerman, J. T.; Himeda, Y.; Fujita, E. *Inorg. Chem.* **2013**, *52*, 12576−12586.

(20) (a) Becke, A. D. *J. Chem. Phys.* **1993**, *98*, 5648−5652. (b) Chengteh, L.; Weitao, Y.; Parr, R. G. *Phys. Rev. B: Condens. Matter* **1988**, *37*, 785−789.

(21) (a) Cundari, T. R.; Stevens, W. J. *J. Chem. Phys.* **1993**, *98*, 5555−5565. (b) Stevens, W. J.; Krauss, M.; Basch, H.; Jasien, P. G. *Can. J. Chem.* **1992**, *70*, 612−630.

(22) Marenich, A. V.; Cramer, C. J.; Truhlar, D. G. *J. Phys. Chem. B* **2009**, *113*, 4538−4543.

(23) Pratt, L. M.; Merry, S.; Nguyen, S. C.; Quan, P.; Thanh, B. T. *Tetrahedron* **2006**, *62*, 10821−10828.
(24) Frisch, M. J. G. *Gaussian 09, Revision D.01*; Gaussian, Inc.: Wallingford, CT, 2009.
(25) NBO analysis was performed using the NBO Version 3.1, as implemented in the Gaussian 09 package by Glendening, E. D.; Badenhoop, J. K.; Reed, A. E.; Carpenter, J. E.; Weinhold, F.
(26) Wang, W. H.; Muckerman, J. T.; Fujita, E.; Himeda, Y. *ACS Catal.* **2013**, *3*, 856−860.
(27) Legault, C. Y. *CYLview, version 1.0*; Université de Sherbrooke, 2009. http://www.cylview.org (accessed July 20, 2014).
(28) Clapham, S. E.; Hadzovic, A.; Morris, R. H. *Coord. Chem. Rev.* **2004**, *248*, 2201−2237.
(29) Simanko, W.; Sapunov, V. N.; Schmid, R.; Kirchner, K.; Wherland, S. *Organometallics* **1998**, *17*, 2391−2393.
(30) Wang, W. H.; Hull, J. F.; Muckerman, J. T.; Fujita, E.; Himeda, Y. *Energy Environ. Sci.* **2012**, *5*, 7923−7926.
(31) (a) Camaioni, D. M.; Schwerdtfeger, C. A. *J. Phys. Chem. A* **2005**, *109*, 10795−10797. (b) Topol, I. A.; Tawa, G. J.; Burt, S. K.; Rashin, A. A. *J. Phys. Chem. A* **1997**, *101*, 10075−10081.
(32) Yang, X. *Dalton Trans.* **2013**, *42*, 11987−11991.
(33) Wasserman, H. J.; Kubas, G. J.; Ryan, R. R. *J. Am. Chem. Soc.* **1986**, *108*, 2294−2301.
(34) Kubas, G. J. *Chem. Rev.* **2007**, *107*, 4152−4205.